PLOS ONE

RESEARCH ARTICLE

Bronchoalveolar lavage affects thorax computed tomography of healthy and SARS-CoV-2 infected rhesus macaques (*Macaca mulatta*)

Annemiek Maaskant[1], Lisette Meijer[1], Zahra Fagrouch[1], Jaco Bakker[1], Leo van Geest[1], Dian G. M. Zijlmans[1], Babs E. Verstrepen[1], Jan A. M. Langermans[1,2], Ernst J. Verschoor[1], Marieke A. Stammes[1]*

1 Biomedical Primate Research Centre (BPRC), Rijswijk, Netherlands, **2** Department Population Health Sciences, Division Animals in Science and Society, Faculty of Veterinary Medicine, Utrecht University, Utrecht, Netherlands

* stammes@bprc.nl

Citation: Maaskant A, Meijer L, Fagrouch Z, Bakker J, van Geest L, Zijlmans DGM, et al. (2021) Bronchoalveolar lavage affects thorax computed tomography of healthy and SARS-CoV-2 infected rhesus macaques (*Macaca mulatta*). PLoS ONE 16(7): e0252941. https://doi.org/10.1371/journal.pone.0252941

Editor: Pierre Roques, CEA, FRANCE

Received: January 28, 2021

Accepted: May 25, 2021

Published: July 9, 2021

Data Availability Statement: All relevant data are within the manuscript and its S1 and S2 Figs, S1–S3 Tables and S1–S8 Videos.

Funding: The author(s) received no external funding for this work.

Competing interests: The authors have declared that no competing interests exist.

Abstract

Medical imaging as method to assess the longitudinal process of a SARS-CoV-2 infection in non-human primates is commonly used in research settings. Bronchoalveolar lavage (BAL) is regularly used to determine the local virus production and immune effects of SARS-CoV-2 in the lower respiratory tract. However, the potential interference of those two diagnostic modalities is unknown in non-human primates. The current study investigated the effect and duration of BAL on computed tomography (CT) in both healthy and experimentally SARS-CoV-2-infected female rhesus macaques (*Macaca mulatta*). In addition, the effect of subsequent BALs was reviewed. Thorax CTs and BALs were obtained from four healthy animals and 11 experimentally SARS-CoV-2-infected animals. From all animals, CTs were obtained just before BAL, and 24 hours post-BAL. Additionally, from the healthy animals, CTs immediately after, and four hours post-BAL were obtained. Thorax CTs were evaluated for alterations in lung density, measured in Hounsfield units, and a visual semi-quantitative scoring system. An increase in the lung density was observed on the immediately post-BAL CT but resolved within 24 hours in the healthy animals. In the infected animals, a significant difference in both the lung density and CT score was still found 24 hours after BAL. Furthermore, the differences between time points in CT score were increased for the second BAL. These results indicate that the effect of BAL on infected lungs is not resolved within the first 24 hours. Therefore, it is important to acknowledge the interference between BAL and CT in rhesus macaques.

Introduction

Infection with Severe Acute Respiratory Syndrome Coronavirus 2 (SARS-CoV-2) and the development of coronavirus 2019 (COVID-19) was first described in Wuhan, Hubei Province, China at the end of 2019 [1]. Since then, SARS-CoV-2 spread rapidly across the globe, leading the World Health Organization to officially declare COVID-19 a Public Health Emergency of International Concern by the end of January 2020.

Animal models are important to answer several research questions like infection progress, disease development, and to evaluate prophylactic and therapeutic treatment options. Due to the close resemblance of their physiology and immune system to that of man, non-human primates (NHPs) play a pivotal role in those aforementioned research topics [2–4]. Multiple studies compared several NHP models to identify their suitability for COVID-19 research, and demonstrated that Old World monkeys, like macaques, are susceptible to SARS-CoV-2 infection and develop mild-to-moderate disease [5–8].

Computed tomography (CT) of the thorax and bronchoalveolar lavage (BAL) are diagnostic procedures widely used in clinical pulmonary research and veterinary medicine [9–12]. These techniques are also used in COVID-19 research in NHPs to gain more information and to create a bridge between the human and NHP data [6, 13, 14]. It is known in NHP and human data that bronchoscopy and BAL can induce several pulmonary effects. In addition to alterations in lung mechanics several studies show an increased neutrophilic cell count in BAL fluid after bronchoscopy or lavage [15–20]. However, to the author's knowledge, no literature concerning the effect of BAL on CT is available regarding NHPs.

For SARS-CoV-2, the infection is predominantly found in the respiratory tract. To determine infection and viral load, nasopharyngeal and tracheal swabs are used to sample the upper respiratory tract. With a BAL, samples from the lower respiratory tract can be obtained [12, 21]. BAL fluid can be used both as diagnostic tool and for detailed analysis of the infection. This includes a variety of analytical tests such as cell counts and differential, cytopathologic analysis, and cultures in addition to specific molecular and immunologic diagnostic tests [9]. In COVID-19 research, it is predominantly used to prove the presence of virus locally in the lungs. By combining swabs with a BAL, the majority of the respiratory tract can be screened. BAL as diagnostic procedure proved its value for the collection of airway cells of the lower respiratory tract. Potential drawbacks of the use of BAL could be the possibility of artificial dissemination of SARS-CoV-2 and the impact on the readout of thorax CTs [13]. In addition, Geri *et al*. suggests that when the swabs of the upper respiratory tract and thorax CTs are negative, it is likely that the BAL is negative as well [22]. Others state that BAL has a place in diagnosis of COVID-19 besides swabs and imaging or that, in vaccine testing, BAL is more robust and specific to demonstrate reduction in viral load than in nasal swabs and more specific than the lesions found on thorax CTs [23–25].

COVID-19 infection studies require optimally characterized macaque infection models. We investigated the effect of BAL on thorax CTs of rhesus macaques. Additionally, we determined the timeframe of possible interference as during BAL a part of the instilled saline is left unrecovered in the lungs [12]. Studies performed in dogs and humans demonstrated that retained saline is correlated with an increase in lung opacity on immediate post-BAL CTs [12, 21]. By this the retained saline can mask COVID-19 associated lesions on CT. Ground glass opacities (GGOs), are also characterized by a slight increase in lung opacity and are commonly found during COVID-19. These lesions resembles the effect of retained saline [13, 26].

The aim of this study is to evaluate the time effects and potential impact of subsequent BALs on the visualization and quantification of the lungs with CT in healthy and SARS-CoV-2 infected rhesus macaques to appraise possible differences during a viral infection.

Materials and methods

Animals & procedures

The study consisted of two groups of rhesus macaques; a non-infected group and a SARS-CoV-2 infected group. The study was conducted at the Biomedical Primate Research Centre (BPRC, Rijswijk, The Netherlands). For the non-infected group, four healthy rhesus macaques

Table 1. Timeline of the procedures in healthy, non-infected, animals.

Day	0 (n = 4)	1	2	3	4	5	6	7
procedure	pre-BAL CT	24h CT	pre-BAL CT	24h CT			pre-BAL CT	24h CT
	BAL		BAL				BAL	
	post-BAL CT		post-BAL CT				post-BAL CT	
	4h CT		4h CT				4h CT	

https://doi.org/10.1371/journal.pone.0252941.t001

were included. From each animal, three BAL samples were taken to evaluate potential deleterious effects on the lung by using various thorax CTs. For the infected group 11 macaques were analyzed, derived from three different COVID-19 studies. These animals were selected out of those studies of which a CT was obtained before and 24 hours after a BAL during the active phase of the infection. Moreover, in four infected macaques an additional BAL at day 2 and an additional CT immediately post-BAL was obtained.

As a timeline, for the non-infected animals three BALs were performed; on Day 0, 2 and 6 respectively named, BAL 1, 2 and 3. With each BAL four CTs are obtained; pre-BAL, post-BAL, four hours post-BAL and 24 hours post-BAL (Table 1). For the infected animals one BAL is performed coupled with two CTs: pre-BAL and 24 hours post-BAL. In addition, four of the infected animals underwent a subsequent BAL at day 2, 48 hours after the first BAL with a pre-BAL CT, post-BAL CT and 24 hours post-BAL CT Table 2).

All animals were of Indian origin, female rhesus macaques (*Macaca mulatta*), purpose bred at the BPRC. During the study the animals were socially housed in pairs. All animals were between 7 and 16 years old and weighed between 6.2 to 11.5 kg. Cages for each pair of animals measured 1 x 2 x 2 meters and were divided into different compartments that were freely accessible to allow animals the choice where to sit. All cages were provided with bedding to allow foraging, environmental enrichment such as fire hoses, mirrors and toys. Daily, all animals also received additional food enrichment items. All procedures, husbandry, and housing performed in this study were in accordance with the Dutch laws on animal experimentation and the regulations for animal handling as described in EU Directive 63/2010. BPRC is accredited by the Association for Assessment and Accreditation of Laboratory Animal Care (AAALAC) International. The study was performed under a project license issued by the Competent Authorities (Central Committee for Animal experiments, license no. AVD5020020209404). Before the start of the study, approval was obtained, by the institutional animal welfare body (CCD 028 Evaluation of vaccines and antiviral compounds against emerging coronavirus infections).

The procedures were all performed in the morning. All macaques were fasted overnight before the procedure while water was freely available throughout. Animals were anesthetized in their home cage with ketamine (10 mg/kg, ketamine hydrochloride, Ketamine 10%; Alfasan Nederland BV, Woerden, the Netherlands) combined with medetomidine hydrochloride (0.05 mg/kg, Sedastart; AST Farma B.V., Oudewater, the Netherlands) intramuscular (IM) and were transferred to the CT-room. At the end of the procedures, when the macaques returned to

Table 2. Timeline of the procedures in the infected animals (<10 dpi) including the additional procedures in 4 infected animals.

Day	0 (n = 11)	1	2 (n = 4)	3
procedure	pre-BAL CT	24h CT	pre-BAL CT	24h CT
	BAL		BAL	
	post-BAL CT		post-BAL CT	

https://doi.org/10.1371/journal.pone.0252941.t002

their home cage, atipamezole (0.25 mg/kg, Sedastop; AST Farma B.V., Oudewater, the Netherlands) was administered IM. In addition, during every sedation bodyweight was measured. It is a standard procedure to fast the animals at least overnight to prevent vomiting and risk of aspiration pneumonia. Afterwards they will receive additional food to recuperate, no weight loss was observed in the animals during the experiment. In addition, the same procedures were used for both non-infected and infected macaques.

Bronchoalveolar lavage

Fiber-optic bronchoscopy (FOB) with BAL targeting the left lung was performed at various time points. The procedure was executed as described before [27]. In brief, a pediatric fiberoptic bronchoscope with a biopsy channel (Karl Storz SE & Co KG, working length 85 cm, outer diameter 5,2 mm, inner diameter working channel 2,3 mm, Tuttlingen, Germany) was used to perform the BAL procedure. The bronchoscope was trans-orally inserted into to trachea and was further manipulated, passing the carina into the left primary bronchus, further into the right secondary bronchus and finally the distal end of the scope was gently wedged in a subsegmental bronchus. A second operator attached the syringe with fluid to the extension tube (Heidelberger Extension, 75 cm, Fresenius Kabi AG, Homburg Germany) placed on the bronchoscope. Three volumes of 20 ml of prewarmed sterile 0.9% saline solution (NaCl 0.9%; B. Braun medical B.V., Oss, the Netherlands) were consecutively instilled in the left lung and subsequently aspirated. In all cases at least 85% of the fluid was recovered. After BAL, the animals were transported to the CT-room, located next to the BAL-room, where the CT was immediately obtained. For the time between the subsequent scans, the animals were transferred back to their home cage.

Computed tomography

Non-invasive, free breathing, CT data were acquired on several time points, including a pre-infection time point, using a MultiScan Large Field of View Extreme Resolution Research Imager (LFER) 150 PET-CT (Mediso Medical Imaging Systems Ltd., Budapest, Hungary). The macaques were positioned head first supine (HFS) with the arms up and fixated in a vacuum pillow. A single CT of the thorax takes 35 seconds by which respiratory motion is inevitable. To mitigate the impact of respiratory motion and improve the image quality, respiratory gating was applied. The respiratory amplitude was detected with a gating pad placed next to the umbilicus. For the final reconstruction, the inspiration phases were exclusively used and manually selected [28].

Gating post-processing is a manual classification of the raw projection data into two phases: silent and motion. Silent phase takes from the end-inspiration to the start-expiration in one respiratory cycle. Motion phase is the remaining part of the cycle. In general, three rotations are sufficient to reach a silent phase of around 95% leaving only a minimal amount of artifacts left. However, the number of repetitions needed depends on the breathing pattern and the delay time between consecutive scans and can be different for each animal and each scan. As the gating is applied retrospectively this can only be partly detected upfront by the number of breathings per minute.

The acquisition parameters used are, 80kVp; 480 projections, an exposure time of 90 msec and 3 or 4 rotations of 360˚. CT image reconstructions were carried out using filtered back projection (FBP) with a RamLak filter, voxel size and slice thickness are 321 μm. Additionally, an adaptive bilateral post filter and a strong unsharp mask are applied to enhance the sharpness and remove noise.

For five of the SARS-CoV-2 infected animals, the 24 hours post-BAL CT was part of a PET-CT procedure. This procedure is described elsewhere [29].

SARS-CoV-2 infection

A group of 11 animals was exposed to a dose of 1 x 10^5 $TCID_{50}$ SARS-CoV-2, diluted in phosphate buffered saline (PBS). The virus was inoculated via a combination of the intratracheal route and intranasal route. During the infection period the animals were checked twice daily by the animal caretakers and scored for clinical symptoms. All animals used in this project had a confirmed SARS-CoV-2 infection as determined by multiple positive qRT-PCR (S1 Table). qRT-PCR was performed as described elsewhere [30, 31]. The clinical and pathological data will be described separately.

Data analysis

CT scoring. A semi-quantitative scoring system for thorax CT evaluation was used to estimate SARS-CoV-2-induced lung disease [7, 13]. Quantification of the opacities on the CTs was performed independently by two experienced imaging scientists based on the sum of the lobar scores. The degree of involvement in each zone was scored as: 0 for no involvement, 1 for <5%, 2 for 5–24%, 3 for 25–49%, 4 for 50–74% and 5 for > = 75% involvement. This scoring system solely looks to the percentage of involvement of each lobe and does not differentiate between different types of lesions like crazy paving patterns, GGOs or consolidations. The only thing which is considered next to the involvement is the difference in density of a lesion of two subsequent scans. When this is increased or decreased but the level of involvement stays the same the score is increased or decreased with 0.5 point. By using this scoring system, a maximum score of 35 could be reached for the combined lobes per time point.

Lung density. In each CT, in two representative planes, in the coronal direction, regions of interest (ROIs) were manually drawn over the left and right lung with a slice thickness of 12 mm using Vivoquant v4.5 (InVicro, Boston, USA). The first ROI is defined in the coronal plane visualizing the trajectory of the bronchoscope into the left lung. The carina is located in the same coronal plane and known to be a relative stable reference point in that area. The second ROI is 50 mm ventral from the first ROI which will end up around the heart. Additionally, when dividing the lungs in a ventral and dorsal part each ROI is in the center of a part. In this way the ROIs are in all lungs defined in the same manner with as less bias as possible. Of those ROIs a histogram was generated representing the voxel intensity, measured in Hounsfield units (HUs) ranging from -1000 to 0. HUs are linearly correlated with physical density and in this way alterations in the lung density pattern after BAL could be visualized. For analyses the histogram was divided into three parts; -1000/-600, -600/-400, and -400/0, which were defined as low density (LD), medium density (MD) and high density (HD), respectively. The LD represents healthy lung based on the average value of the non-infected animals. The HD represents non-healthy lung tissue and the MD as intermediate, in this range the differences between scans were also captured due to the normal existing differences in respiratory amplitude and pattern. Afterwards absolute values were converted to relative values to compensate for the difference in lung volume both between scans and between animals and calculated as area under the curve (AUC).

Statistical analysis. Statistical tests were performed with SPSS statistics v26 and GraphPad prism v8.4.2. After testing for normal distribution, the t-test was used to compare the results obtained from the histograms and the Wilcoxon signed-rank test for CT scores. For correlation analysis, respectively a Pearson and Spearman correlation were applied. The level of significance was $\alpha = 0.05$, all tests were performed two-sided and where possible paired.

Results

Before comparing the different groups and timepoints with each other, the entire group of animals (n = 4 (non-infected), 11 (infected)) was examined for possible confounding factors in relation to age and weight. In correlation with both visual and quantitative assessment no confounding factors were found for these parameters.

Visual assessment non-infected group

In all non-infected animals, an increase in density was visible in the lavaged lung around the opening of the main bronchus at the CT performed immediately post-BAL. The increased density was more focused in either the middle or the lower lobe. Overall, the spread of the BAL fluid was more in the dorsal direction of the lungs than the ventral direction. At the scan obtained four hours post-BAL, the majority of the alterations observed immediately post-BAL were resolved. In addition, the density of the lesions was decreased. At the scan obtained 24 hours after the BAL, the lungs had visually returned to baseline values obtained just before BAL. This pattern was similar in all animals which received a BAL. The timeline and representative CT images of one animal are visualized in Fig 1 and in S1–S4 Videos.

The individual scores pre-/post-BAL of the CT images on the different time points are summarized in Fig 2 and S2 Table. Due to a technical problem, one of the non-infected animals was lavaged in the right lung instead of the left. This animal was excluded from further data analysis.

The average difference in CT score for the left lung between the pre-BAL CT and the CT obtained after 24 hours was 0.2, confirming that at 24 hours post-BAL the appearance of the lungs is comparable to the pre-BAL situation. Nevertheless, when comparing the subsequent BALs with each other, the CT score pre-BAL 2 and four hours post-BAL 2 were higher compared to the related time points of BAL 1 and BAL 3.

Post-BAL the left lung scored between 8–11, a significantly higher score compared to all pre-BAL time points ($p<0.001$). Four hours post-BAL, the CT scores in the left lung where still increased but the difference was no longer significant ($p = 0.19$). Additionally, post-BAL two animals showed a positive CT score in the right lung but had returned to baseline values at four hours post-BAL. At two time points a positive CT score in the right lung was observed at the CT 24 hours post-BAL, the reason for this is unclear.

Quantitative assessment non-infected group

In Fig 3, the histograms of a representative animal (RM 3) are visualized. These histograms illustrate the relative HU value, and with this density of the lungs, in all time points. In S1 and S2 Figs. RM1 and RM2 are visualized. In all graphs the line representing the post-BAL CT can be clearly distinguished from the other plots. In addition, the peak of the 24h post-BAL CT peak is for all animals and all BALs similar or even less dense compared to the pre-BAL CT.

There was a significant difference for all three BALs visible at the post-BAL CT for the left lung for both the LD and HD range; LD (decrease in AUC of 30.6%, $p = 0.003$), HD (increase in AUC of 86.7%, $p = 0.001$). At four hours post-BAL, this difference was still significant compared to the pre-BAL values, now also for the MD range (decrease in AUC of 10.0%, $p = 0.026$), but the AUC change reversed for both LD (increase in AUC of 16.5%, $p = 0.014$) and HD (decrease in AUC of 14.4%, $p = 0.012$) for the left lung. There were also differences found in the right lung, for the four hour timepoint, for the entire histogram; LD (increase in AUC of 11.5%, $p = 0.012$), MD (decrease in AUC of 19.8%, $p = 0.026$), HD (decrease in AUC of 9.4%, $p = 0.079$). For 24 hours post-BAL, no significant differences were observed.

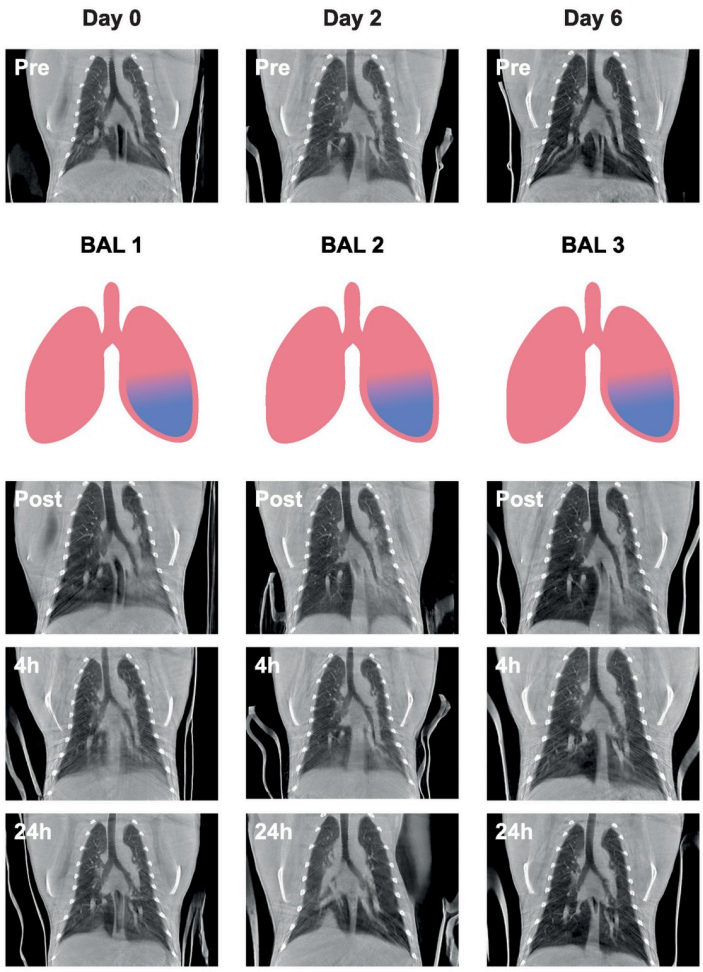

Fig 1. Representative coronal slices (of RM2) of all CTs obtained during the three BALs. The procedures are represented in a vertical manner whereas the time in days is represented horizontally. The procedure starts with a pre-BAL CT (Pre), followed by a left-sided (blue) BAL 1, a post-BAL CT (Post) and a four hour post-BAL CT (4h) on Day 0. The next day, Day 1, the 24 hour post-BAL CT (24h) was obtained. The procedures for BAL 2 and BAL 3 were performed in a similar order.

https://doi.org/10.1371/journal.pone.0252941.g001

Visual assessment SARS-CoV-2 infected group

In Fig 4, representative pre-BAL CT and 24 hours post-BAL CT cross sections are shown of two animals, while infected with SARS-CoV-2. The lesions found in the animal visualized in the upper row (RM 2) were minimal and slightly increased on the 24 hours post-BAL time point (S5 and S6 Videos). For the animal visualized in the bottom row (RM 8), the density of both lungs was increased. For the left lung multiple consolidations were observed on the 24 hours post-BAL CT. On the left side the entire lung, predominantly dorsal, was affected whereas on the pre-BAL CT the majority of the lesions were found in the lower lobe in combination with a GGO in the upper lobe. In addition, in the right lung moderate lesions were detected (S7 and S8 Videos).

In line with the SARS-CoV-2 infection all animals had a positive CT score in at least one side of the lung at the pre-BAL time point. In these animals the CT score of the left lung 24 hours post-BAL was significantly increased ($p = 0.007$) compared to pre-BAL CT score with a positive correlation ($r = 0.907$ $p<0.0001$). For the right lung this difference was not observed.

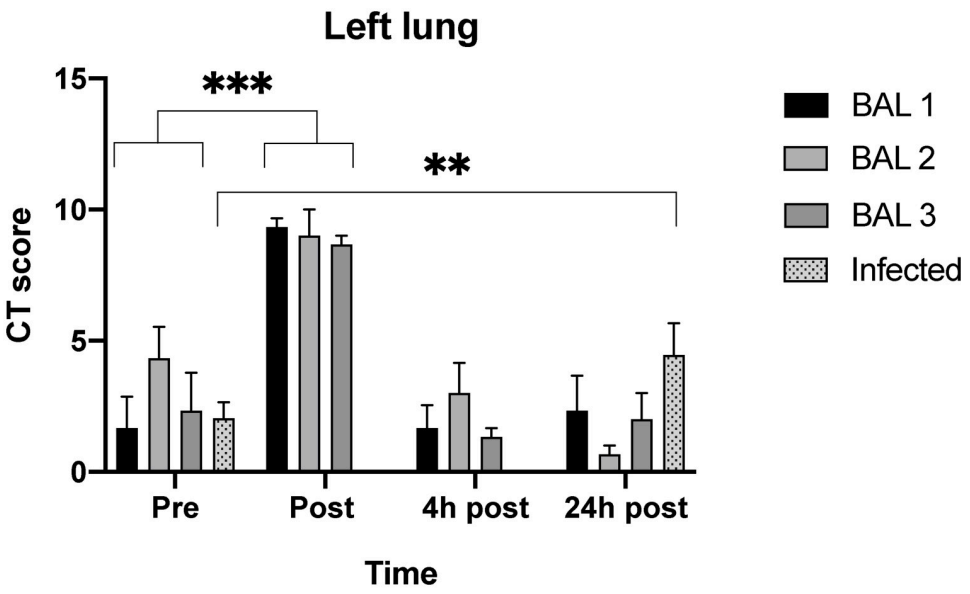

Fig 2. Average CT scores of the left lung of both non-infected (n = 3) and infected (n = 11) macaques. For the non-infected group, the average CT scores of the four timepoints are represented for BAL 1, 2 and 3. As for the SARS-CoV-2 infected group the average CT scores of the two timepoints are represented. Post-BAL 1, 2 and 3 the CT scores of the non-infected group were significantly higher compared to pre-BAL 1, 2 and 3. The infected group showed a significant increase in post-BAL CT score compared to pre-BAL. Values are mean ± SEM, Wilcoxon signed-rank test was performed; ** $p<0.01$, *** $p<0.001$.

https://doi.org/10.1371/journal.pone.0252941.g002

The individual scores of these infected macaques are summarized in Fig 2 and S3 Table. As previously described a daily CT score of 35 can be reached for the entire lung with a maximum of 15 and 20 for the left and right lung, respectively.

Quantitative assessment SARS-CoV-2 infected group

In Fig 5, the histograms of two representative SARS-CoV-2-infected animals are visualized. These histograms illustrate the relative AUC for the HU values, and with this density of the lungs of the CT obtained before BAL and 24 hours after BAL.

A significant increase in AUC (19.4%) was found for the right lung in the LD range ($p = 0.004$) and a significant decrease in AUC (16.6%) in the MD range ($p = 0.002$). For the left lung a significant difference was only found in the HD range (increase in AUC of 23.2%, $p = 0.016$).

Comparison BAL 1 versus BAL 2

To investigate the impact of subsequent BALs obtained within a time range of a couple of days, we had seven animals (three non-infected and four infected) from which two BALs were taken within 48 hours (Fig 6). A significant difference in AUC, for the left lung, at the pre-BAL 2 CT was found for both the LD range (decrease in AUC of 27.3%, $p = 0.022$) and MD range (increase in AUC of 18%, $p = 0.010$) and a trend within the HD range (increase in AUC of 55.2%, $p = 0.076$). Also, for the CT score a significant increase was observed for the left lung ($p = 0.016$) at this pre-BAL 2 time point compared to the pre-BAL 1 time point. To explore whether there were differences in the CT scores between the time points in both BALs, the CT scores were subtracted from their respective pre-BAL CT score. In this way, a significant

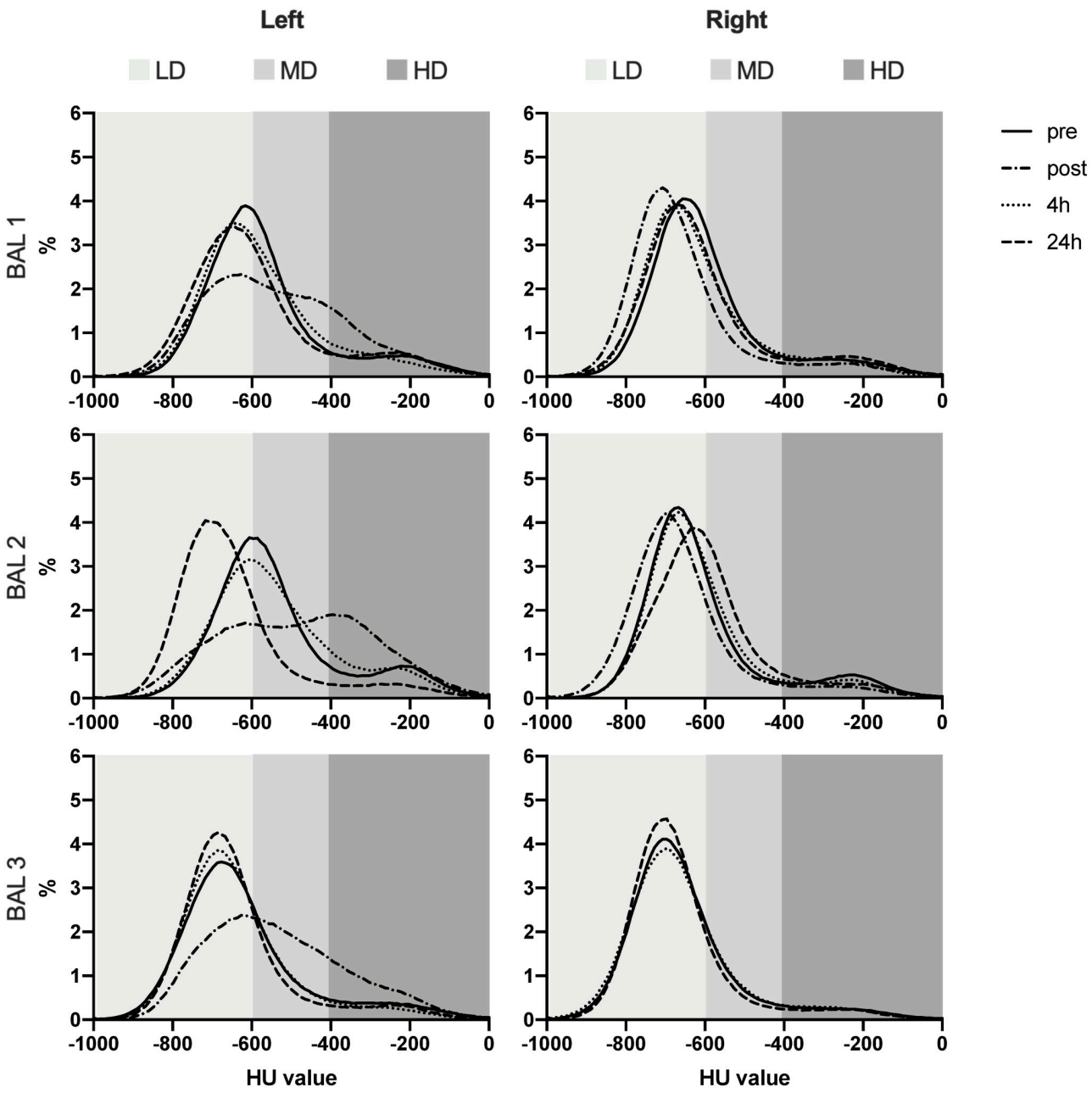

Fig 3. Histograms representing the relative lung density pattern of the left and right lung of one representative (RM3) of the non-infected group. LD = -1000/-600 HU, healthy lung, MD = -600/-400 HU, HD = -400/0 HU, non-healthy lung.

https://doi.org/10.1371/journal.pone.0252941.g003

increase in CT score was found for the left lung for the post-BAL time point of BAL 1 versus BAL 2 (p = 0.047) and for the 24 hours post BAL time point of BAL 1 versus BAL 2 (p = 0.031). In addition, for these values a positive correlation was found (r = 0,77). These differences, for the 24 hours post BAL time point, were also detected for all ranges of the histogram; LD (p = 0.023), MD (p = 0.042) and HD (p = 0.015). For the right lung, no significant differences were found for lung density and CT scores or subtracted scores.

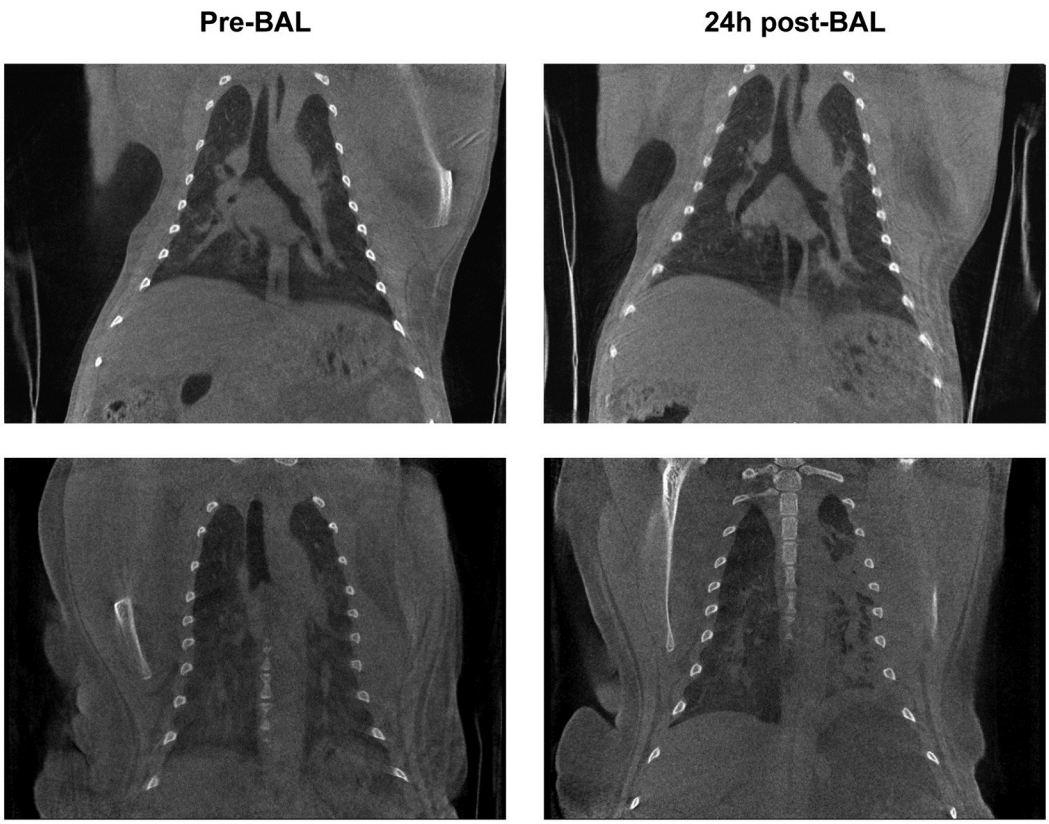

Fig 4. CTs of two infected animals. Upper row RM2; bottom row RM8. Pre-BAL on the left side, and 24 hours post-BAL on the right.

https://doi.org/10.1371/journal.pone.0252941.g004

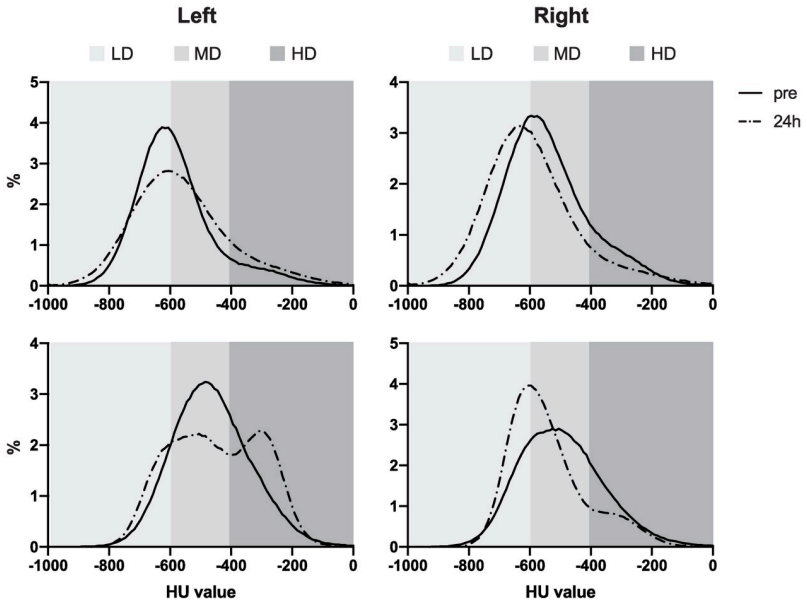

Fig 5. Histograms representing the relative lung density pattern of the left and right lung of SARS-CoV-2 infected macaques.

https://doi.org/10.1371/journal.pone.0252941.g005

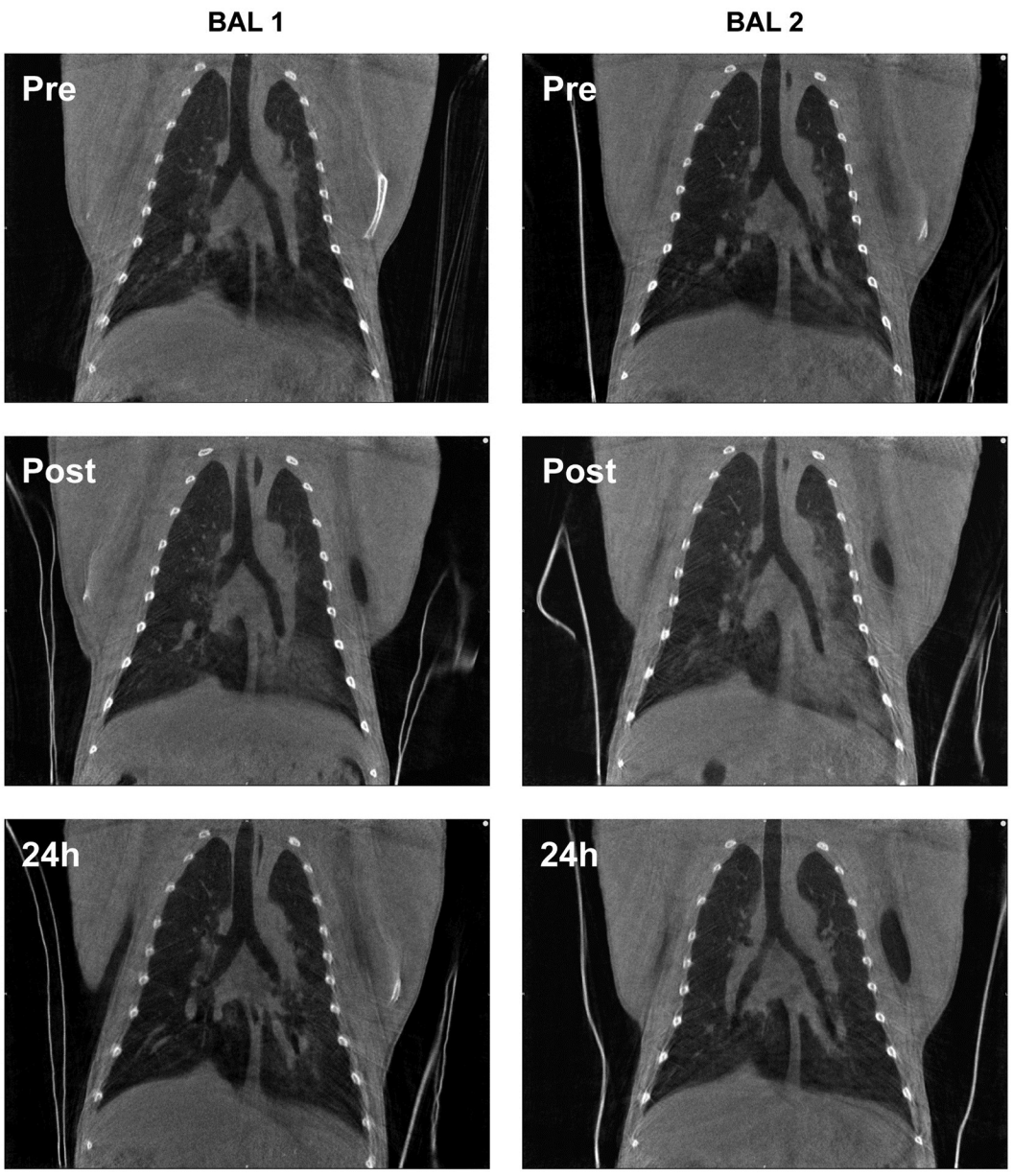

Fig 6. Representative coronal CT slices of the first and second BAL of a SARS-CoV-2 infected rhesus macaque (RM3).

https://doi.org/10.1371/journal.pone.0252941.g006

Discussion

In infectious lung diseases, both CT and BAL are valuable diagnostic modalities which are often included in preclinical and clinical research. However, the possible interference of BAL on CT has not been investigated, so far, in NHPs. The findings in this study demonstrate that, thorax CT alterations due to BAL seem to be resolved within 24 hours in non-infected macaques. However, for SARS-CoV-2 infected animals, significant differences for both the semi-quantitative CT score and quantitative AUCs were found at the 24 hours post-BAL CT. In addition, the effect of the second BAL within 48 hours of the first BAL shows significant alterations, supporting the idea that the effect of the BAL is not finished after 24 hours and therefore might influence acquired CT data.

The pulmonary changes induced by BAL fluid were most pronounced on the immediate post-BAL CT. On those images, increased radiographic opacities were found due to the BAL procedure. The majority of these opacities decreased within four hours after BAL and returned to normal within 24 hours after the procedure. Despite differences in BAL procedure, the changing opacities in time after BAL seen in the macaques are comparable to results obtained in humans and dogs [12, 21]. In both studies, a known amount of unrecovered BAL fluid was left in the lung, bilateral in humans and unilateral in dogs. In addition, in dogs no aspiration or repeated instillation was performed. In the current study, the procedure was similar to commonly used BAL techniques including repeated fluid instillation and subsequent aspirations. Moreover, as the amount of fluid recovered was similar for all BAL procedures there is no correlation between these two. The average weight of our animals was 8.7 kg and the retained saline after BAL was maximal 9 ml, 15% of the instilled fluid, resulting in a comparable amount retained saline as installed volume (1 ml/kg) used in dogs [12]. In this study the pulmonary changes returned to normal within 24 hours. These findings are in that regard similar to our findings in the non-infected animals. The differences in pre-BAL CT are therefore most likely due to nature of the retrospective gating procedure. We aim for a silent rate, in the inspiration phase, as high as possible and at least above 90%. The higher the silent rate in the inspiration phase the less motion and expiration phase is incorporated in the scan. During expiration the lungs will become denser as they contain less air, in this regard a silent rate of 90% will probably lead to a slight shift in density to the right (denser) compared to a scan with a silent rate of 95%. Unfortunately, it is impossible to circumvent this fully as the breathing pattern and amount of breathings per minute differ for each animal.

As for the findings in the right lung, the CT score immediately post-BAL was possibly caused by redistribution or a spill of the retained saline due to a change of body posture or by coughing [21]. This was supported by the fact that at four hours post-BAL no alterations were found in the right lung anymore. An explanation for the CT score found 24 hours post-BAL remains unclear. However, a possible explanation could be, as stated by Cohen and Batra, that bronchoscopy alone could initiate effects in the contralateral lung [32].

The current study does not provide evidence of an increased percentage of retained fluid but redistribution between the lung lobes due to coughing cannot be excluded. The differences found between BAL 1 and BAL 2 suggest that the effect of these procedures is still ongoing 24 hours after subsequent BALs, however not clearly visible. As BAL 3 was obtained four days after BAL 2, it was not expected to find ongoing effects that could be related to BAL 2. After comparing all the outcome parameters from BAL 1 with BAL 3 and BAL 2 with BAL 3 significant differences were not found.

Multiple publications showed that NHPs are susceptible to SARS-CoV-2 infection and develop a mild-to-moderate form of disease, with the discrimination made between mild and moderate based on the presence or absence of imaging findings [5–8, 33]. In the current study, the majority of the infected animals (10/11) showed CT scores above zero at the pre-BAL timepoint. In addition, infection with SARS-CoV-2 was confirmed in each animal by qRT-PCR. The strong positive correlation that was found between the pre-BAL and 24 hour post-BAL CT scores indicates that a BAL can potentially enhance the visual pathology of infected lung tissue. As COVID-19 is a rapidly developing infection it cannot be excluded that the increase in CT score is due to a disease aggravation. However, in patients fluctuations in thorax CT abnormalities are not observed during the active phase of the infection. The active phase can be divided in four stages; early (day 0–5), progressive (day 5–8), peak (day 9–13) and late stage ($\geq$ 14 days) suggesting a Gaussian curve in the temporal evolution of lung abnormalities [34]. This is supported by the observation during multiple studies at our facility, that SARS-CoV-2 infected rhesus macaques show an equal or even lower score in subsequent CTs obtained over

24 hours after BAL though before ten days post infection. The current study suggests that these fluctuations found are induced by the BAL as all scans are obtained within the first ten days of infection. In addition, by now we have infected over hundred animals, both rhesus macaques and cynomolgus macaques, with SARS-CoV-2 in multiple studies. The time frame in which viral RNA was detectable varied from only one day to up to ten days in macaque. The individual variation of SARS-CoV-2 RNA levels detected in the macaques was, regardless of species, considerable. The same is true for the manifestation of lung lesions, the individual variation is considerable. Moreover, no correlation could be detected between viral load in the swabs and CT score.

Furthermore, the right lung showed less lesions compared to the left lung. As the number of lesions reflected by the CT score seems to influence the outcome this may be of impact. Since the infection with SARS-CoV-2 went by intratracheal and intranasal route it was expected that both lungs would reveal a similar CT score. However, in the animals included in this study, the left lung showed more lesions compared to the right lung. An unexpected finding, as this was not observed in other SARS-CoV-2 infection studies performed at our institute. What was observed is the high level of heterogeneity between the animals in the infectious take of SARS-CoV-2. This is probably coincidence as our animal selection was solely based on availability of BALs coupled with CTs.

As expected, the animals showed an increase in HD range of the left lung, caused by the remnants of the BAL fluid. More interestingly, an increase in the LD range in their non-lavaged right lung was found. Amigoni *et al.* showed in mice, that the relative tidal volume of the contralateral lung of an injured lung increased while mechanical ventilated [35]. These data support the hypothesis that the contralateral lung will develop a coping mechanism to ensure sufficient oxygenation. The AUC decrease in LD and MD versus increase in HD immediate post-BAL can be explained by the instillation of relative HD saline. These findings are in corroboration with the measured post-BAL non-air volumes in humans [21]. At four hours post-BAL, the reversed significant difference, compared to the pre-BAL values for both LD and HD for the left lung, could probably be explained as a similar compensating reaction described above to the initial loss of LD tissue in the lavaged lobe of the lung. This assumption can neither be confirmed nor completely denied with the limited amount of data available on this topic. Further research on lobar regions with more subjects is necessary to confirm these findings.

Another objective was to investigate the impact of multiple BALs on CT. Therefore, we compared BAL 1 and BAL 2, performed within 48 hours in seven animals. It was interesting to find a difference in AUC, for the left lung, in all ranges. These findings confirm the impact of the BAL on the recovery time based on the readout of thorax CTs when multiple BALs are performed in a short period of time [13]. As four animals in this group were infected, although unlikely, artificial dissemination of SARS-CoV-2 cannot be excluded. Krombach et al. demonstrated that serial BALs do not cause major damage to bronchoalveolar structures in healthy experimental macaques despite the known neutrophile influx [18, 20, 32]. Although BAL is widely used, some pulmonary effects elicited by a BAL procedure are still unclear. For example, the mechanism of increased pulmonary compliance post-BAL is not established [17]. In addition, the exact fate of the BAL fluid is uncertain [21]. In general, it is most likely that the retained saline in the alveoli is absorbed by the interstitial space and will be transported in the pulmonary lymphatics or pulmonary capillaries). However, it is plausible that the SARS-CoV-2 infection impairs the normal drainage mechanism of the lung. Histopathology of SARS-CoV-2 infected macaques show interstitial and alveolar infiltration alveolar damage and thickening and histological changes in pulmonary lymph nodes [36, 37]. These pulmonary impairments could be an explanation for the incapacity to clear the lungs from the BAL effects in the

SARS-CoV-2 infected animals at a similar rate as the non-infected animals. Resulting in an increased lung density and CT score for a longer period of time compared to the non-infected animals.

Whereas the discussion concerning the diagnostic value of both BAL and CT in human is ongoing, there is consensus of the value of both procedures in COVID-19 NHP models [6, 13, 14, 21, 24, 25]. The current study shows that when using both BAL and CT it is important to acknowledge the existing interference between those two valuable techniques in rhesus macaques.

Supporting information

S1 Table. Viral load in samples of SARS-CoV-2 infected macaques.
(DOCX)

S2 Table. Overview of the CT scores of the non-infected macaques.
(DOCX)

S3 Table. Overview of the CT scores of SARS-CoV-2 infected macaques.
(DOCX)

S1 Fig. Histogram RM 1.
(DOCX)

S2 Fig. Histogram RM 2.
(DOCX)

S1 Video. CT Videos of representative non-infected animal at four timepoints.
(MP4)

S2 Video. CT Videos of representative non-infected animal at four timepoints.
(MP4)

S3 Video. CT Videos of representative non-infected animal at four timepoints.
(MP4)

S4 Video. CT Videos of representative non-infected animal at four timepoints.
(MP4)

S5 Video. CT Videos pre-BAL and 24 hours post-BAL RM 2.
(MP4)

S6 Video. CT Videos pre-BAL and 24 hours post-BAL RM 2.
(MP4)

S7 Video. CT Videos pre-BAL and 24 hours post-BAL RM 8.
(MP4)

S8 Video. CT Videos pre-BAL and 24 hours post-BAL RM 8.
(MP4)

Acknowledgments

We would like to thank the Animal Science Department, especially the animal caretakers for excellent care of the animals, Francisca van Hassel for her assistance with figure editing and both the virology and parasitology department for performing the SARS-CoV-2 infection studies.

Author Contributions

Conceptualization: Annemiek Maaskant, Ernst J. Verschoor, Marieke A. Stammes.

Formal analysis: Annemiek Maaskant, Lisette Meijer, Zahra Fagrouch, Dian G. M. Zijlmans, Babs E. Verstrepen, Marieke A. Stammes.

Methodology: Annemiek Maaskant, Lisette Meijer, Zahra Fagrouch, Jaco Bakker, Leo van Geest, Babs E. Verstrepen, Marieke A. Stammes.

Supervision: Jan A. M. Langermans, Marieke A. Stammes.

Writing – original draft: Annemiek Maaskant, Lisette Meijer, Marieke A. Stammes.

Writing – review & editing: Annemiek Maaskant, Lisette Meijer, Jaco Bakker, Dian G. M. Zijlmans, Babs E. Verstrepen, Jan A. M. Langermans, Ernst J. Verschoor, Marieke A. Stammes.

References

1. Chan JF, Yuan S, Kok KH, To KK, Chu H, Yang J, et al. A familial cluster of pneumonia associated with the 2019 novel coronavirus indicating person-to-person transmission: a study of a family cluster. Lancet. 2020; 395(10223):514–23. https://doi.org/10.1016/S0140-6736(20)30154-9 PMID: 31986261
2. Matute-Bello G, Frevert CW, Martin TR. Animal models of acute lung injury. Am J Physiol Lung Cell Mol Physiol. 2008; 295(3):L379–99. https://doi.org/10.1152/ajplung.00010.2008 PMID: 18621912
3. Estes JD, Wong SW, Brenchley JM. Nonhuman primate models of human viral infections. Nat Rev Immunol. 2018; 18(6):390–404. https://doi.org/10.1038/s41577-018-0005-7 PMID: 29556017
4. Cleary SJ, Pitchford SC, Amison RT, Carrington R, Robaina Cabrera CL, Magnen M, et al. Animal models of mechanisms of SARS-CoV-2 infection and COVID-19 pathology. Br J Pharmacol. 2020; 177(21):4851–65. https://doi.org/10.1111/bph.15143 PMID: 32462701
5. Lu S, Zhao Y, Yu W, Yang Y, Gao J, Wang J, et al. Comparison of nonhuman primates identified the suitable model for COVID-19. Signal Transduct Target Ther. 2020; 5(1):157. https://doi.org/10.1038/s41392-020-00269-6 PMID: 32814760
6. Kumar Singh D. SARS-CoV-2 infection leads to acute infection with dynamic cellular and inflammatory flux in the lung that varies across nonhuman primate species. bioRxiv. 2020.
7. Böszörményi KPS M.A.; Fagrouch Z.C.; Kiemenyi-Kayere G.; Niphuis H.; Mortier D.; van Driel N; et al. Comparison of SARS-CoV-2 infection in two non-human primate species: rhesus and cynomolgus macaques. bioRxiv. 2020.
8. Johnston SC. Development of a Coronavirus Disease 2019 Nonhuman Primate Model Using Airborne Exposure. bioRxiv. 2020.
9. Davidson KR, Ha DM, Schwarz MI, Chan ED. Bronchoalveolar lavage as a diagnostic procedure: a review of known cellular and molecular findings in various lung diseases. J Thorac Dis. 2020; 12(9):4991–5019. https://doi.org/10.21037/jtd-20-651 PMID: 33145073
10. Hoffman AM. Bronchoalveolar lavage: sampling technique and guidelines for cytologic preparation and interpretation. Vet Clin North Am Equine Pract. 2008; 24(2):423–35, vii–viii. https://doi.org/10.1016/j.cveq.2008.04.003 PMID: 18652963
11. Johnson LR, Vernau W. Bronchoalveolar lavage fluid lymphocytosis in 104 dogs (2006–2016). J Vet Intern Med. 2019; 33(3):1315–21. https://doi.org/10.1111/jvim.15489 PMID: 30912207
12. Lim S, Sung S, Min K, Jung Y, Cho Y, Lee K. Bronchoalveolar lavage affects computed tomographic and radiographic characteristics of the lungs in healthy dogs. Vet Radiol Ultrasound. 2018; 59(5):564–70. https://doi.org/10.1111/vru.12656 PMID: 29931791
13. Finch CL, Crozier I, Lee JH, Byrum R, Cooper TK, Liang J, et al. Characteristic and quantifiable COVID-19-like abnormalities in CT- and PET/CT-imaged lungs of SARS-CoV-2-infected crab-eating macaques (Macaca fascicularis). bioRxiv. 2020.
14. Hartman AL, Nambulli S, McMillen CM, White AG, Tilston-Lunel NL, Albe JR, et al. SARS-CoV-2 infection of African green monkeys results in mild respiratory disease discernible by PET/CT imaging and shedding of infectious virus from both respiratory and gastrointestinal tracts. PLoS Pathog. 2020; 16(9):e1008903. https://doi.org/10.1371/journal.ppat.1008903 PMID: 32946524

15. Haley PJ, Muggenburg BA, Rebar AH, Shopp GM, Bice DE. Bronchoalveolar lavage cytology in cynomolgus monkeys and identification of cytologic alterations following sequential saline lavage. Vet Pathol. 1989; 26(3):265–73. https://doi.org/10.1177/030098588902600312 PMID: 2763415

16. Kazmierowski JA, Gallin JI, Reynolds HY. Mechanism for the inflammatory response in primate lungs. Demonstration and partial characterization of an alveolar macrophage-derived chemotactic factor with preferential activity for polymorphonuclear leukocytes. J Clin Invest. 1977; 59(2):273–81. https://doi.org/10.1172/JCI108638 PMID: 401834

17. Klein U, Karzai W, Zimmermann P, Hannemann U, Koschel U, Brunner JX, et al. Changes in pulmonary mechanics after fiberoptic bronchoalveolar lavage in mechanically ventilated patients. Intensive Care Med. 1998; 24(12):1289–93. https://doi.org/10.1007/s001340050764 PMID: 9885882

18. Krombach F, Fiehl E, Burkhardt D, Rienmuller R, Konig G, Adelmann-Grill BC, et al. Short-term and long-term effects of serial bronchoalveolar lavages in a nonhuman primate model. Am J Respir Crit Care Med. 1994; 150(1):153–8. https://doi.org/10.1164/ajrccm.150.1.8025742 PMID: 8025742

19. Rennard SI, Ghafouri M, Thompson AB, Linder J, Vaughan W, Jones K, et al. Fractional processing of sequential bronchoalveolar lavage to separate bronchial and alveolar samples. Am Rev Respir Dis. 1990; 141(1):208–17. https://doi.org/10.1164/ajrccm/141.1.208 PMID: 2297178

20. Von Essen SG, Robbins RA, Spurzem JR, Thompson AB, McGranaghan SS, Rennard SI. Bronchoscopy with bronchoalveolar lavage causes neutrophil recruitment to the lower respiratory tract. Am Rev Respir Dis. 1991; 144(4):848–54. https://doi.org/10.1164/ajrccm/144.4.848 PMID: 1928961

21. Gabe LM, Baker KM, van Beek EJ, Hunninghake GW, Reinhardt JM, Hoffman EA. Effect of segmental bronchoalveolar lavage on quantitative computed tomography of the lung. Acad Radiol. 2011; 18 (7):876–84. https://doi.org/10.1016/j.acra.2011.03.006 PMID: 21669353

22. Geri P, Salton F, Zuccatosta L, Tamburrini M, Biolo M, Busca A, et al. Limited role for bronchoalveolar lavage to exclude COVID-19 after negative upper respiratory tract swabs: a multicentre study. Eur Respir J. 2020; 56(4). https://doi.org/10.1183/13993003.01733-2020 PMID: 32764117

23. Vannucci J, Ruberto F, Diso D, Galardo G, Mastroianni CM, Raponi G, et al. Usefulness of bronchoalveolar lavage in suspect COVID-19 repeatedly negative swab test and interstitial lung disease. J Glob Antimicrob Resist. 2020; 23:67–9. https://doi.org/10.1016/j.jgar.2020.07.030 PMID: 32810641

24. Aggarwal D, Saini V. Factors limiting the utility of bronchoalveolar lavage in the diagnosis of Covid-19. Eur Respir J. 2020. https://doi.org/10.1183/13993003.03116-2020 PMID: 32859675

25. Mercado NB, Zahn R, Wegmann F, Loos C, Chandrashekar A, Yu J, et al. Single-shot Ad26 vaccine protects against SARS-CoV-2 in rhesus macaques. Nature. 2020; 586(7830):583–8. https://doi.org/10.1038/s41586-020-2607-z PMID: 32731257

26. Warman A, Warman P, Sharma A, Parikh P, Warman R, Viswanadhan N, et al. Interpretable Artificial Intelligence for COVID-19 Diagnosis from Chest CT Reveals Specificity of Ground-Glass Opacities. medRxiv. 2020. https://doi.org/10.1101/2020.05.16.20103408 PMID: 32511545

27. Singletary ML, Phillippi-Falkenstein KM, Scanlon E, Bohm RP Jr., Veazey RS, Gill AF. Modification of a common BAL technique to enhance sample diagnostic value. J Am Assoc Lab Anim Sci. 2008; 47 (5):47–51. PMID: 18947171

28. Tölgyesi BB, J.; Nagy, K.; van Geest, L.; Stammes, M.A. Refined acquisition of high-resolution thorax CTs in macaques by free breathing 2020.

29. Stammes MA B J.; Vervenne R.A.W.; Zijlmans D.G.M.; van Geest L.; Vierboom M.P.M.; Langermans J. A.M.; et al. Recommendations for Standardizing Thorax PET–CT in Non-Human Primates by Recent Experience from Macaque Studies Animals. 2021; 11(1). https://doi.org/10.3390/ani11010204 PMID: 33467761

30. Corman VM, Landt O, Kaiser M, Molenkamp R, Meijer A, Chu DK, et al. Detection of 2019 novel coronavirus (2019-nCoV) by real-time RT-PCR. Euro Surveill. 2020; 25(3).

31. Wolfel R, Corman VM, Guggemos W, Seilmaier M, Zange S, Muller MA, et al. Virological assessment of hospitalized patients with COVID-2019. Nature. 2020; 581(7809):465–9. https://doi.org/10.1038/s41586-020-2196-x PMID: 32235945

32. Cohen AB, Batra GK. Bronchoscopy and lung lavage induced bilateral pulmonary neutrophil influx and blood leukocytosis in dogs and monkeys. Am Rev Respir Dis. 1980; 122(2):239–47. https://doi.org/10.1164/arrd.1980.122.2.239 PMID: 6774640

33. Zu ZY, Jiang MD, Xu PP, Chen W, Ni QQ, Lu GM, et al. Coronavirus Disease 2019 (COVID-19): A Perspective from China. Radiology. 2020; 296(2):E15–E25. https://doi.org/10.1148/radiol.2020200490 PMID: 32083985

34. Kwee TC, Kwee RM. Chest CT in COVID-19: What the Radiologist Needs to Know. Radiographics. 2020; 40(7):1848–65. https://doi.org/10.1148/rg.2020200159 PMID: 33095680

35. Amigoni M, Bellani G, Zambelli V, Scanziani M, Farina F, Fagnani L, et al. Unilateral acid aspiration augments the effects of ventilator lung injury in the contralateral lung. Anesthesiology. 2013; 119(3):642–51. https://doi.org/10.1097/ALN.0b013e318297d487 PMID: 23681142

36. Fahlberg MD, Blair RV, Doyle-Meyers LA, Midkiff CC, Zenere G, Russell-Lodrigue KE, et al. Cellular events of acute, resolving or progressive COVID-19 in SARS-CoV-2 infected non-human primates. Nature Communications. 2020; 11(16078). https://doi.org/10.1038/s41467-020-19967-4 PMID: 33247138

37. Zheng H, Li H, Guo L, Liang Y, Li J, Wang X, et al. Virulence and pathogenesis of SARS-CoV-2 infection in rhesus macaques: A nonhuman primate model of COVID-19 progression. PLoS Pathog. 2020; 16(11):e1008949. https://doi.org/10.1371/journal.ppat.1008949 PMID: 33180882